

Phase transitions of copper, aluminum, and tungsten wires during underwater electrical explosions

A. Rososhek,¹ S. Efimov,¹ S. V. Tewari,¹ D. Yanuka,² and Ya. E. Krasik¹

¹Physics Department, Technion, Haifa 3200003, Israel

²Plasma Physics Group, Imperial College London, London SW7 2BW, United Kingdom

(Received 26 July 2018; accepted 10 October 2018; published online 29 October 2018)

Using streak images of underwater electrically exploding copper, aluminum, and tungsten wires (current densities of 10^7 – 10^8 A/cm² and energy density deposition of 10–50 kJ/g) and generated weak shocks, the onset of each phase transition, its duration, and the time when the wire explosion occurred were determined. The measured discharge current and resistive voltage were used to calculate the energy and energy density deposition. Using the discharge current waveform and the onset of the strong shock wave, the specific action integral was calculated and compared with published data. The thermodynamic parameters during the wire explosion were calculated using one-dimensional magneto-hydrodynamic simulations coupled with equations of state for water, copper, and aluminum. It was shown that the onset times of weak shocks, in general, cannot be related to the melting or the evaporation of the entire wire. *Published by AIP Publishing.*

<https://doi.org/10.1063/1.5049904>

I. INTRODUCTION

Electrical explosions of wires in water are a promising method for exploring the properties of warm dense matter,¹ which are important for the verification of conductivity models and equations of state (EOS) at extreme conditions. The wire explosion is accompanied by solid → liquid → vapor → plasma phase transitions along which the electrical and thermodynamic parameters change within a broad range. During the last few decades, intensive research was carried out with wires made of different conducting materials subjected to electrical pulses with current densities of 10^6 – 10^9 A/cm² and durations of 10^{-5} – 10^{-9} s, exploding in different background media (vacuum, gas, and liquid).^{2–7} It was shown that depending on the current density, different modes of wire explosions can be obtained, i.e., “slow” explosion ($j \leq 10^7$ A/cm²) when magneto-hydrodynamic (MHD) instabilities have enough time to develop or, for significantly larger current densities, “fast” explosions, characterized by the development of thermal instabilities.^{8–12} For fast explosions, if the skin time is significantly shorter than the current rise time, the explosion can be considered volumetric. On the other hand, an explosion is considered “superfast,” when the skin-layer thickness is much smaller than the wire radius. The latter is realized on nanosecond time scale explosions with current densities $>10^8$ A/cm². The structure of exploding wires was studied using either laser based diagnostics¹³ or soft x-ray backlighting.¹⁴ For instance, in vacuum, using a sub-nanosecond scale soft x-ray pinch as a backlighter point, it was shown¹⁴ that electrical explosion in vacuum of wires made of refractory and highly resistive metals results in the formation of a foam like liquid-vapor structure and part of the wire remains in a condensed state.

The energy density deposition rate, wire material, and background medium also affect the radial expansion rate of the wire. For a gas background, a fast decrease in density

can result in current interruption, leading to large induced voltage generation during the vapor-plasma phase transition during up to several tens of nanoseconds. Also, for fast wire explosions in gas/vacuum, it is very challenging to prevent the formation of surface flashover, leading to the generation of a plasma which carries part of the discharge current.^{15,16} In order to avoid this surface flashover, Sarkisov *et al.*¹³ studied ns-timescale electrical explosions in vacuum of wires with $2 \mu\text{m}$ dielectric coating. It was shown that this coating suppressed the radial expansion of the exploding wire and the formation of the flashover can be avoided, at least before the evaporation of the dielectric layer.

Electrical explosion of wires was simulated using semi-empirical models based on self-similarity parameters^{17–19} and MHD numerical modeling^{20–32} coupled with EOS^{33–35} and conductivity models.^{36–40} The results of such numerical modeling showed that because of fast heating ($>10^9$ K/s), the liquid and vapor phases can coexist and that the time-dependent conductivity cannot be considered to be uniform along the wire’s cross section. Also, MHD numerical modeling showed that one has to modify the EOS and the conductivity model in order to reproduce the experimentally obtained current and the resistive voltage waveforms and the radial expansion of the wire.

Underwater electrical explosions of wires^{17,18,22–24,31,41–44} have several advantages when compared to wire explosions in vacuum or gas. The water environment prevents the formation of plasma along the wire’s surface, typical of electrical wire explosions in vacuum or gas. The discharge is then critically damped, and most of the energy stored in the pulse generator is deposited into the wire during a time shorter than a quarter-period of the harmonic oscillations obtained for a short-circuit load. This leads to the formation of a low-ionized high-resistivity plasma with a coupling coefficient $\Gamma > 1$. Moreover, due to the low compressibility of water, the energy density deposition in underwater electrical explosion is high, that is, the radial

expansion of the exploding wire in water is significantly slower ($\leq 2.5 \times 10^5$ cm/s) than in gas/vacuum ($\sim 10^7$ cm/s). Nevertheless, the radial expansion of the exploding wire during the phase of the main energy deposition, when low-ionized plasma forms, leads to the generation of strong shock waves (SW) with pressures over 10^9 Pa.

The absence of parasitic surface plasma and the almost negligible radial expansion of the wire prior to its explosion allows one to study solid-liquid-vapor phase transitions by visualization of weak shocks, the formation of which should be related to the onset of these transitions. In earlier experiments^{45,46} of underwater electrical wire explosions, weak shocks in water were observed. It was suggested that the onset of these shocks corresponds to phase transitions of the exploding wires; however, a detailed analysis of the energy density deposited into the wire prior to these events and their relation to the energy required for complete phase transitions was not performed.

In this paper, we present the results of experiments of electrical explosions of copper (Cu), aluminum (Al), and tungsten (W) wires in water. The main focus of the present study was to determine the onset of the phase transitions using high-resolution shadow streak images of the wire explosion during the generated shocks. These data were compared with the energy density deposition calculated using the measured discharge current and resistive voltage and with the results of one dimensional (1D) MHD simulations. These streak images were also used to define the time of the explosion which, in turn, was used to calculate the specific current action integral which was compared to published data.

II. EXPERIMENTAL SETUP

The experiments were carried out using two μ s-time-scale pulse generators.^{47,48} Each of these generators is based on four low-inductance high-voltage (HV) capacitors, connected in parallel and having a total capacitance of either 0.88 μ F or 9.6 μ F, charged to either 35 kV or to 25 kV, respectively, and discharged by spark gas switches (see Fig. 1). These generators with a stored energy of 0.54 and 3 kJ will be labeled as generators #1 and #2, respectively. The spark gaps of the generators were triggered using Maxwell trigger generators with an output pulse time jitter of ± 2 ns. Prior to the wire explosion experiments, the parameters of the discharge circuit were determined in generator shots with short-circuit loads. It was found that the total inductance and resistance of the discharge circuits were ~ 590 nH/ ~ 65 nH and ~ 0.17 Ω / ~ 0.01 Ω , for generators #1 and #2, respectively, with a comparable oscillation quarter-period of ~ 1200 ns. The maximal discharge current amplitudes, realized in these experiments, were ~ 32 and 180 kA for generators #1 and #2, respectively. 45 mm long, 250 μ m/600 μ m (Cu), 250 μ m/800 μ m (Al), and 200 μ m/700 μ m (W) diameter wires were used for generators #1 and #2, respectively. These wires were exploded with almost critically damped discharges. The total mass of the Cu, Al, and W wires was 0.0198 g/0.114 g, 0.006 g/0.0611 g, and 0.0272 g/0.3334 g, for generators #1 and #2, respectively. The wire was placed

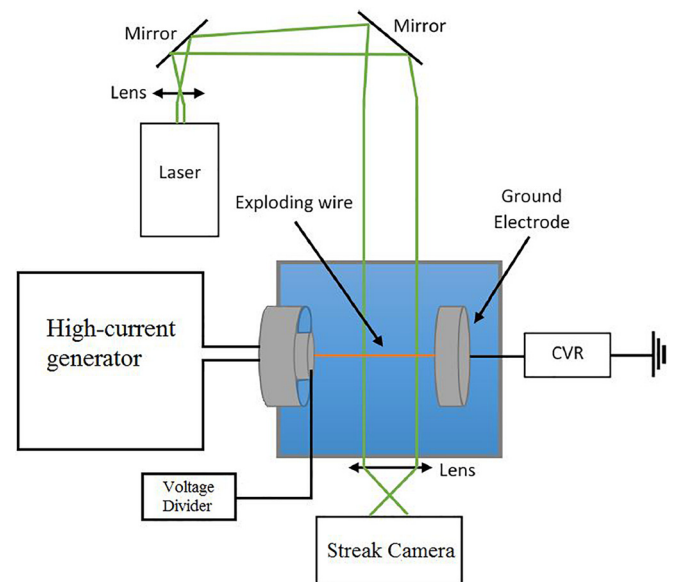


FIG. 1. Typical experimental setup.

in a stainless-steel chamber between the grounded and the HV electrodes and the chamber was filled with tap water (see Fig. 1).

The discharge current through the wire was measured using a low-inductance coaxial current viewing resistor (CVR) of 21 m Ω resistance. The voltage was measured using a Tektronix voltage divider connected to the HV electrode. In experiments with generator #2, the discharge current was measured using a self-integrated Rogowski coil. A 155 mW diode-pumped, 532 nm CW laser (MGL-III-532) and a single mode 532 nm, 2.5 W, CW laser (by Roithner Lasertechnik GmbH) were used to backlight the exploding wire and the SW. The shadow images of the exploding wires and generated shocks were recorded using a streak camera (Optoscope SC-10) operating with streak durations in the range 0.5–2 μ s. To synchronize between the generator shot time and the streak camera, a Stanford Digital Delay Generator DG645 was used. The error in the measured time interval between the streak image starting time and the beginning of the discharge current was found to be ± 15 ns.

At least four generator #1 and two generator #2 shots were carried out for each wire material, sufficient for reproducibility in the waveforms of the discharge current and voltage and repeatable shadow images of the exploding wire and the generated shocks. The error in calculating the experimentally obtained energy density deposition into the exploding wires was estimated as $\pm 3\%$ and was related to the spatial and time resolution of the streak shadow images and errors in the current calibration ($\pm 3\%$ for CVR and $\pm 10\%$ for Rogowski coil) and the voltage ($\pm 1\%$) probes.

III. EXPERIMENTAL RESULTS

Typical waveforms of the current, resistive voltage, time evolution of the wire's resistance, and deposited power and energy for Cu, Al, and W wire explosions are shown in Fig. 2. One can see that the explosion of wires is characterized by an almost critically damped discharge. For Cu and

Al wire explosions, the current amplitude reached ~ 30 kA with ~ 900 ns rise time, and the resistive voltage was $\phi_r = \phi_w - (L_w + L_0)dI/dt \approx 35$ kV, where L_w and L_0 are the inductances of the wire and the grounded electrode, respectively, I is the current, and ϕ_w is the measured voltage. The energy deposition rate for Al wire explosions was significantly higher than for Cu wires. This is because of the use of a non-optimal diameter of the Cu wire, resulting in a late explosion (~ 890 ns, compared to ~ 780 ns for Al), smaller resistive voltage, and smaller wire maximum resistance when compared to Al wire explosions. Nevertheless, the total deposited energy $\epsilon = \int_0^t I(t)\phi_r(t)dt$ and maximal power $P = I(t)\phi_r(t)$ differed by only $\sim 15\%$ for both explosions for which the main parameters are shown in Table I.

For W wire explosions, the waveforms of the discharge current and resistive voltage were very different from those of Cu and Al (see Fig. 2). The maximum amplitude of the discharge current was smaller by a factor of ~ 2 compared to those of Cu or Al. Also, similarly to earlier work,^{22,24,41} a relatively long plateau in the discharge current (~ 400 ns) and voltage (~ 700 ns) is obtained. The resistance of the W wire increases fast to $\sim 1.7 \Omega$, and it does not change significantly during ~ 650 ns. These electrical parameters suggest that for W, the durations of the phase transitions experienced by the W wire during its explosion are different.

The average current densities at maximum current for Cu, Al, and W wire explosions were close to each other, $j_{\text{Cu}} \approx 6.5 \times 10^7$ A/cm², $j_{\text{Al}} \approx 5.7 \times 10^7$ A/cm², and $j_{\text{W}} \approx 4.5 \times 10^7$ A/cm², respectively. However, the energy density deposition into the wires was different, namely, 18.9 kJ/g (13 eV/atom), 53.7 kJ/g (15 eV/atom), and 10.1 kJ/g (19 eV/atom) for Cu, Al, and W wires, respectively. The values of the specific current actions,^{3,7} derived from energy conservation, are the property of the exploding material, $h = \int_0^{\tau} j^2(t')dt'$, where j is the current density, t is the time, and τ is the time of explosion determined from the streak image of the exploding wire and the waveform of the discharge current when the latter reaches its maximal amplitude. Using this definition and accounting for the radial expansion of Cu, Al, and W wires, the values of h were found to be 1.3×10^9 A² s/cm⁴, 0.75×10^9 A² s/cm⁴, and 0.6×10^8 A² s/cm⁴, respectively. The values of h are similar to the values in Refs. 6–8 (except for W wire explosions) for current densities $j \leq 5 \times 10^7$ A/cm² (see Table II).

Typical shadow streak images of exploding Cu, Al, and W wires and the generated shocks are shown in Fig. 3. The spatial and temporal resolution of these images is $3.37 \mu\text{m}/\text{pixel}$ and 0.72 ns/pixel for Cu and Al wires, respectively, and $3.37 \mu\text{m}/\text{pixel}$, 1.44 ns/pixel for W wires. One can see weak shocks generated slightly before and during the maximum of

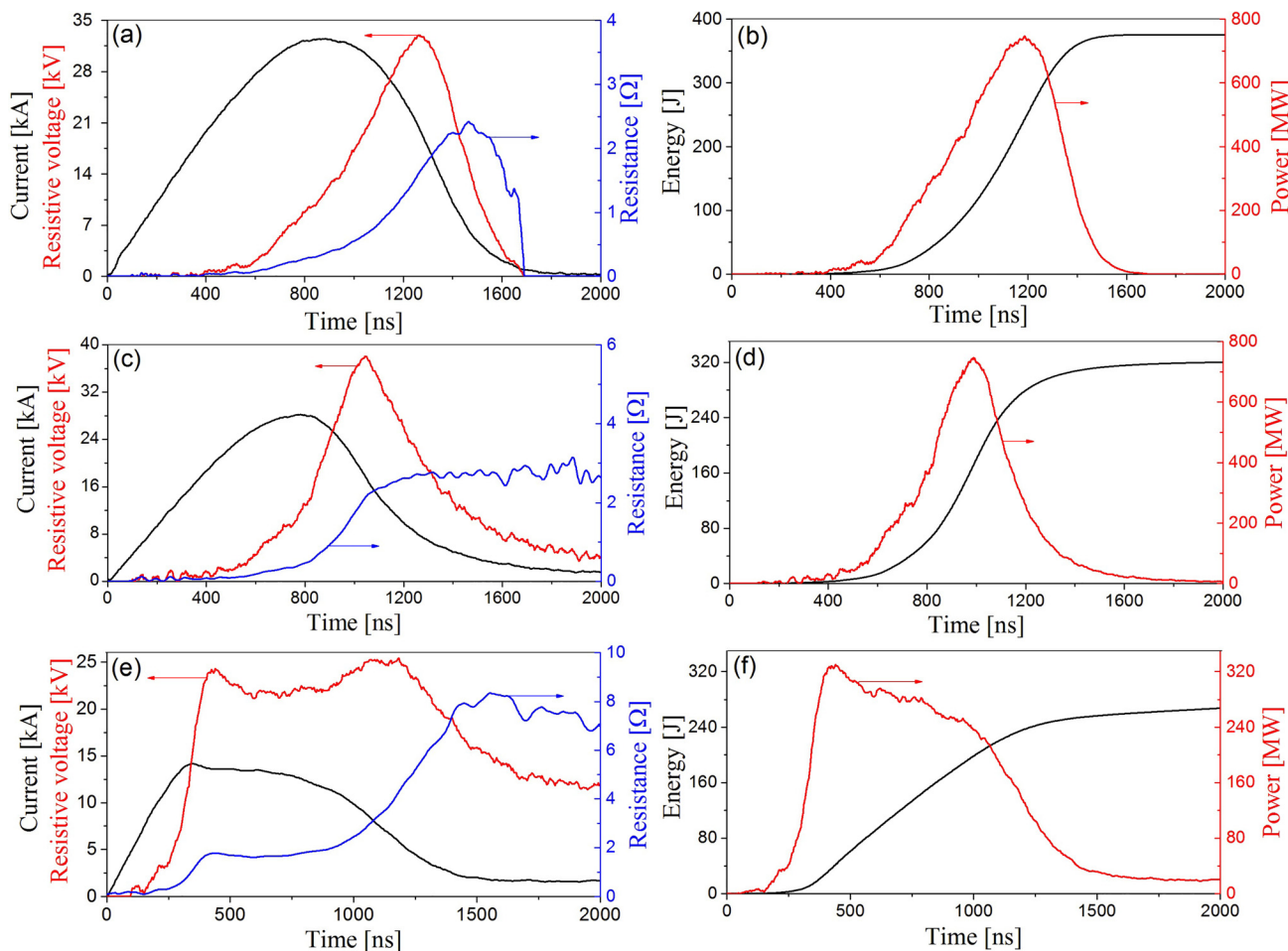


FIG. 2. Waveforms of the discharge current, resistive voltage, and time-dependent resistance obtained in explosions of Cu (a), Al (c), and W (e) wires. Power and energy deposition for Cu (b), Al (d), and W (f) wire explosions.

TABLE I. Electrical parameters for Cu and Al wire explosions in water. Errors of 3% and 1% in the current and voltage measurements, respectively. Errors in deposited energy, resistance, and power were computed using quadrature of the current and voltage errors.

Material	Current rise-time (ns)	Maximal current amplitude (kA)	Maximal resistive voltage amplitude (kV)	Resistance at maximal voltage (Ω)	Deposited energy (J)	Maximal power (MW)
Copper	880	32.0 ± 1.0	33.0 ± 0.3	1.6 ± 0.2	376 ± 11	750 ± 25
Aluminum	780	28.0 ± 0.8	38.0 ± 1.2	2.1 ± 0.4	320 ± 9	750 ± 25
Tungsten	350	14.0 ± 0.5	25.0 ± 0.8	4.3 ± 0.5	275 ± 8	330 ± 10

the discharge current, propagating with velocities exceeding the speed of sound in water by 10% to 15% as shown in Table III. We assume that these weak shocks were generated at the onset of the phase transitions caused by rapid Joule heating of the wires. The onset times of the weak shocks relative to the beginning of the discharge current and their velocities are shown in Table III.

The velocities of the weak shocks were calculated using a linear approximation of the shock trajectory obtained using the streak shadow images. The error in these calculations was found to be ± 20 m/s for all wire materials and was related to the shock front blur of ~ 6 pixels in both vertical and horizontal directions. The propagation velocity of the 3rd shock was not calculated due to difficulties in determining this trajectory on the streak image.

Assuming that the onset of the 1st and 2nd weak shocks can be related to the melting and the evaporation of the wires accompanied by a fast change in volume, one can calculate the energy density deposited into the wires at those times. These experimental data can be compared with the tabulated data,⁴⁹ using temperature dependent heat capacities in both the solid and liquid phases. We assume that the skin effect, MHD, and thermal instabilities¹¹ have little influence on the radial uniformity of the energy deposition, which is indeed the case for generator #1 and not quite so for generator #2, but both cases will be addressed in Sec. IV. The results of this comparison are shown in Table IV. The 1st and 5th columns represent the deposited energy densities $\epsilon_1 = m_w^{-1} \int_0^{t_1} I(\tau) \phi_r(\tau) d\tau$ and $\epsilon_3 = m_w^{-1} \int_{t_1}^{t_2} I(\tau) \phi_r(\tau) d\tau$, where m_w is the mass of the wire and t_1 and t_2 are the onsets of the 1st and 2nd weak shocks, respectively. The 2nd and 6th columns represent the energy densities $\epsilon_2^* = C_V(T_m - T_0)$ and $\epsilon_4^{**} = C_V(T_b - T_m)$ required to heat the wire from room temperature, T_0 , to its melting T_m and boiling T_b temperatures, respectively. The values of the specific heat capacities in the solid phase for Cu, Al, and W as a function of temperature were used from Refs. 50 and 51. In the liquid phase, according to Ref. 50, the specific heat capacity measured at constant pressure can be considered constant for these metals. Thus, the values of heat capacities

in the liquid phase were found by extrapolating the ratio between the isochoric and isobaric heat capacities obtained in the solid phase and the values of the isobaric heat capacity in the liquid phase.⁴⁹ The values $\Delta\epsilon_{12} = \epsilon_1 - \epsilon_2^*$ and $\Delta\epsilon_{34} = \epsilon_3 - \epsilon_4^{**}$, which are expected to be the latent heat (enthalpy of fusion or evaporation) required for solid \rightarrow liquid and liquid \rightarrow vapor phase transitions, are shown in the 3rd and 7th columns of Table IV, respectively. The 4th and 8th columns contain tabulated values⁴⁹ of latent heats for fusion and evaporation, respectively.

The relative errors in the measured discharge current and voltage were added in the 1st and 5th columns. The errors in the 2nd and 6th columns were calculated using data presented in Refs. 50 and 51; the errors in the 3rd and 7th columns were calculated as the quadrature of the errors in 2nd, 3rd, 5th, and 6th columns, respectively.

One can see a different relationship between the deposited energy and the energy required for the solid \rightarrow liquid phase transition of Cu, Al and W wire explosions. For Cu, the energy density of ~ 1220 J/g deposited into the wire prior the onset of the 1st weak shock is larger than the energy density of ~ 580 J/g required to heat the wire to its melting temperature plus the enthalpy of fusion. However, this inequality was not obtained for Al wire explosions, where the measured deposited energy density of ~ 970 J/g is almost equal to the tabulated value for fusion (~ 986 J/g).

For W wire explosions, when the 1st weak shock has set on, the energy density of ~ 620 J/g deposited into the wire was lower than the energy of ~ 800 J/g, required for the solid-liquid phase transition of the entire wire. This required 800 J/g deposited ~ 20 ns after the first weak shock has separated from the wire. A weak shock seen in Fig. 3(e) at $t \approx 240$ ns was not reproducible in time for different shots. At present we do not have a reasonable explanation for the appearance of this disturbance. We assume that either imperfections in the W wire structure formed during its production, or absorbed gas desorption could be responsible for the generation of this weak shock.

For the vaporization stage of the wire explosions (see columns 5–8, Table IV), one obtains consistent results for all tested wires. Namely, the onset of the 2nd weak shock is obtained when the measured deposited energy density is significantly smaller than the energy density required for the entire wire vaporization. For instance, for Cu wire explosions, in contrast to the melting case, one obtains the onset of the 2nd weak shock when ~ 1.2 kJ/g energy density was deposited instead of ~ 5.9 kJ/g required for total vaporization of the wire. Also, at this stage of the Al wire explosion, an artificial negative value of latent heat $\Delta\epsilon_{34}$ necessary for entire wire vaporization was obtained.

TABLE II. Specific current actions for Al and Cu materials.

	Copper $\text{A}^2 \text{s/cm}^4 \times 10^9$	Aluminum $\text{A}^2 \text{s/cm}^4 \times 10^9$	Tungsten $\text{A}^2 \text{s/cm}^4 \times 10^9$
Reference 6	2.0	0.90	1.8
Reference 7	1.6	0.59	
Reference 8	2.9	1.26	
Present research	1.3	0.75	0.6

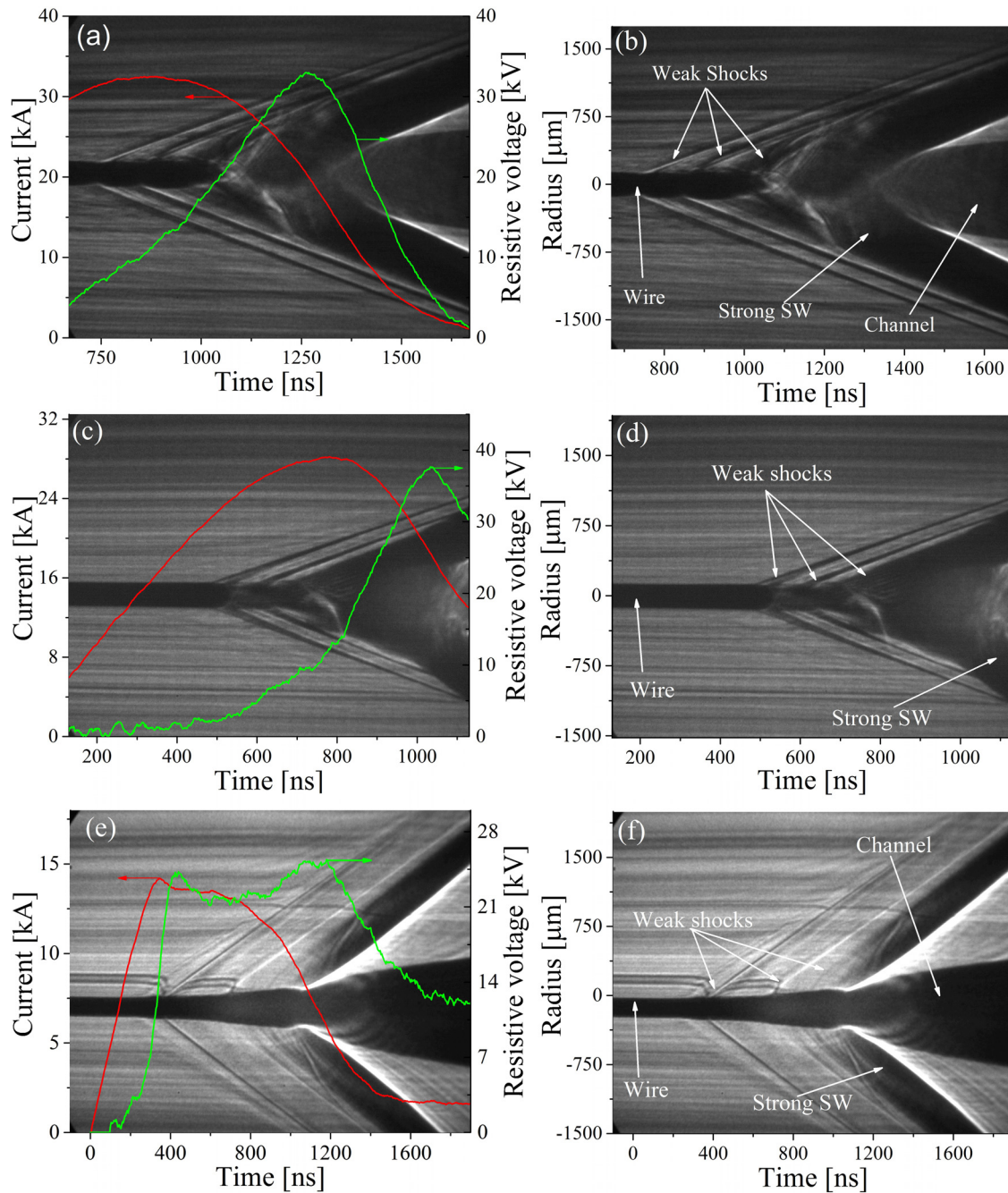


FIG. 3. Typical laser backlit streak images overlapped with the discharge current and resistive voltage waveforms (a), (c), and (e) the same images with spatial and temporal scales (b), (d), and (f). (a) and (b) are for a Cu wire, (c) and (d) an Al wire, and (e) and (f) a W wire explosions.

TABLE III. Weak shock summary.

Wire	Time of the 1st weak shock onset, t_1 (ns)	Shock wave velocity (m/s)	Time of the 2nd weak shock onset t_2 (ns)	Shock wave velocity (m/s)	Time of 3rd weak shock onset t_3 (ns)
Cu	740	1570	800	1630	940
Al	490	1580	600	1690	670
W	360	1680	660	1650	890

IV. DISCUSSION

A. Copper wire explosion

In order to obtain the parameters of the exploding wire, 1D MHD modeling, accounting for thermal diffusion and

coupled with electrical circuit equations, EOS³³ for copper and water, and the BKL conductivity model,³⁶ was carried out. The details of this modeling were described in earlier publications.^{26,32} The input parameters in the simulations were the charging voltage, parameters of the HV generator

TABLE IV. Comparison of the experimentally obtained energy densities deposited into the wire prior to the onset of the 1st and 2nd weak shocks with tabulated data of the energy densities required for melting and evaporation for Cu, Al, and W. *Melting temperatures for Cu, Al, and W are: $T_m^{Cu} \approx 1358\text{K}$, $T_m^{Al} \approx 933\text{K}$, and $T_m^W \approx 3690\text{K}$. **Boiling temperatures for Cu, Al, and W are: $T_b^{Cu} \approx 2833\text{K}$, $T_b^{Al} \approx 2790\text{K}$, and $T_b^W \approx 6200\text{K}$.

Material	1 ϵ_1 (J/g)	2 ϵ_2^* (J/g)	3 $\Delta\epsilon_{12}$ (J/g)	4 ΔH_f (J/g)	5 ϵ_3 (J/g)	6 ϵ_4^{**} (J/g)	7 $\Delta\epsilon_{34}$ (J/g)	8 ΔH_e (J/g)
Copper	1220±35	395±10	830±36	190	740±20	620±10	120±25	5315
Aluminum	970±30	595±30	375±30	390	1300±40	1840±90	-540±100	12230
Tungsten	625±20	545±10	80±20	255	3345±100	400±10	2945±100	4630

and the load. In order to obtain satisfactory matching with experimental data, the pressure and the internal energy in the EOS database, as well as the conductivity values in the conductivity model, were modified in a similar manner to that described in Ref. 27. Namely, two modification approaches were used. Either the values of the pressure were corrected, while keeping the internal energy constant, until best fit with experimental data was obtained; or, the values of the pressure were kept unchanged while the internal energy values were corrected. The results of both methods give similar radial density distribution agreeing with channel expansion. The BKL conductivity model was changed in a similar manner. Namely, first, we identified the time intervals where the reproduction of the current and resistive voltage waveforms was not satisfactory. Then, for these time intervals, the values of conductivity depending on the density and temperature were corrected until the best fit with current and resistive voltage waveforms is obtained. The experimentally obtained and simulated waveforms of the discharge current and resistive voltage are shown in Figs. 4(a) and 4(b), and comparison between experimentally observed and simulated exploding Cu wire radial expansion is shown in Fig. 4(c). Note that during the period of 900–1500 ns, the wire radial expansion cannot be resolved because the generated strong shockwave screens the exploded wire. In Fig. 4(d), the current density radial distribution is shown for different times of the Cu wire explosion. One can see that the skin-effect is significant only during the first ~ 200 ns, whereas later in time the current density radial distribution is almost uniform. This agrees qualitatively with the condition of uniform heating $r_0 \ll \delta_s$, where r_0 is the radius of the wire, and δ_s is the skin layer. This condition is satisfied for the present experimental conditions, accounting for the increase in the skin layer due to Joule heating of the Cu wire.

The results described in Sec. III showed that for Cu wire explosion, the onset of the first weak shock occurs after the energy density needed for solid \rightarrow liquid phase transition was deposited into the wire. In order to explain this result, the temporal evolution of the simulated pressure, temperature, and magnetic pressure at the wire surface is shown in Fig. 5. One can see that the melting temperature for Cu ($T_m^{Cu} \approx 1358\text{K}$) is reached at $t \approx 660$ ns. The measured energy density deposited into the wire at that time is almost equal to the sum of energy density needed to heat the wire up to T_m^{Cu} plus the enthalpy of fusion. However, the departure of the first weak shock wave occurs ~ 80 ns later. This can be related to an interplay between the magnetic and internal pressures, namely, once the melting point is reached, the

internal pressure increases in such a manner that once it exceeds the magnetic pressure the onset of the first weak shock wave is observed. As mentioned above, the diameter of the Cu wire was not optimal for an overdamped discharge. The latter results in the discharge current and resistive voltage maxima occurring later in time than for an Al wire (see Table I), which affects the energy density deposition and the development of the phase transitions.

The experimental results showed that the onset of the second weak shock was at $t \approx 800 \pm 15$ ns. At that time, the deposited energy density reached 740 J/g which is considerably lower than the energy necessary for the complete wire vaporization (~ 5930 J/g). Note that according to the measured energy density deposition, the time when ~ 5930 J/g was obtained is ~ 1040 ns, that is, ~ 240 ns after the onset of the second shock obtained at $t \approx 800$ ns. This can be explained only by the fractional evaporation of the wire. Indeed, the results of the MHD modeling presented in Fig. 6 showed that at $t \approx 800$ ns, the current density is larger in the wire core while at $t \approx 760$ ns, the current density distribution is almost uniform. Thus, one concludes that the resistance at the wire periphery, shown by the red curve in Fig. 6, became larger due to a “vaporization wave” propagating towards the axis and creating the second weak shock, shown in Fig. 3(b).

Let us now address Cu wire explosions carried out using generator #2. The diameter of the wires, 600 μm , was ~ 2.4 times larger than that of the wires used in experiments with generator #1. Streak shadow images showed the onset of the first weak shock at $t \approx 340$ ns (recall that the maximum of the discharge current was obtained at $t_{max} \approx 1100$ ns). At that time, the energy density deposition was only ~ 80 J/g, which is ~ 7 times less than the energy density required to heat the entire wire to its melting temperature plus the enthalpy of fusion. Thus, one can state that this first weak shock wave was generated when only an insignificant part of the wire experienced a solid \rightarrow liquid phase transition. Later in time, namely, at $t \approx 520$ ns and $t \approx 670$ ns, two succeeding weak shocks were obtained. At these times, the deposited energy densities were ~ 360 J/g and ~ 600 J/g, respectively. Let us note that only the third weak shock’s onset corresponds to the time when the deposited energy becomes sufficient for the melting of the entire wire.

The earlier onset of the weak shock differs significantly from the result obtained in experiments with Cu wire explosion using generator #1, where the onset of the first weak shock was obtained at $t \approx 740$ ns when the energy density deposited into the wire exceeded the energy density required to heat the entire wire to the melting temperature plus the

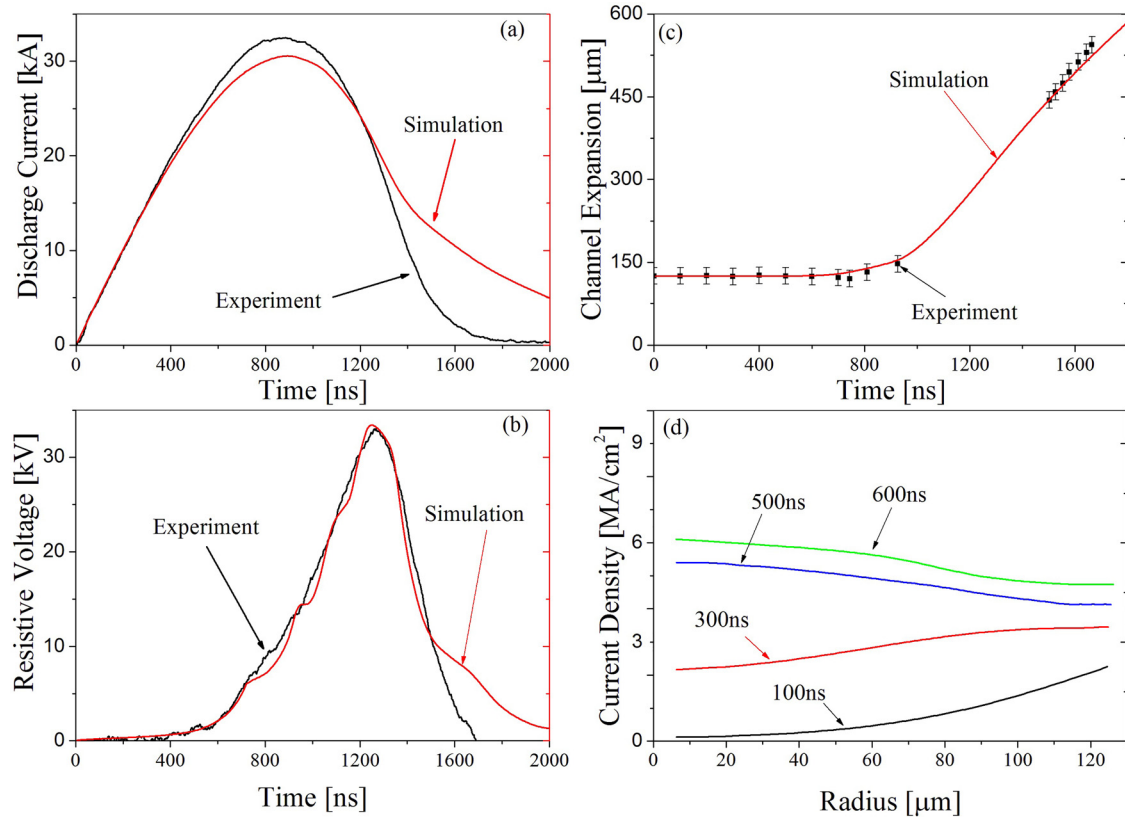


FIG. 4. Experimental and simulated waveforms of the discharge current (a), resistive voltage (b), channel expansion (c) and the simulated current density radial distribution (d) for Cu wire explosion.

enthalpy of fusion. One can consider the skin-effect as a possible explanation for this apparent contradiction. For the case of generator #1, the skin effect (skin layer for normal conductivity is $\sim 65 \mu\text{m}$) is pronounced during only the first ~ 200 ns and later in time one obtains an almost uniform current density radial distribution (see Fig. 4). However, the MHD simulation showed that for generator #2, the current density radial distribution remains non-uniform with larger current density at the periphery of the wire, during the first ~ 500 ns of the discharge. Considering the melting of the

surface layer of the Cu wire and calculating the energy density deposited at the onset of the first shock ($t \approx 340$ ns, ~ 2 J) one obtains the thickness of the melted layers are $\sim 50 \mu\text{m}$. The formation of this melted layer bounded by water and solid copper can lead to the appearance of a weak shock. Namely, the copper's compressibility is significantly lower than that of water, resulting in the generation of weak shocks. The second weak shock obtained during the wire's partial melting can be related to the propagation of the first shock wave in copper towards the wire axis and reflection.

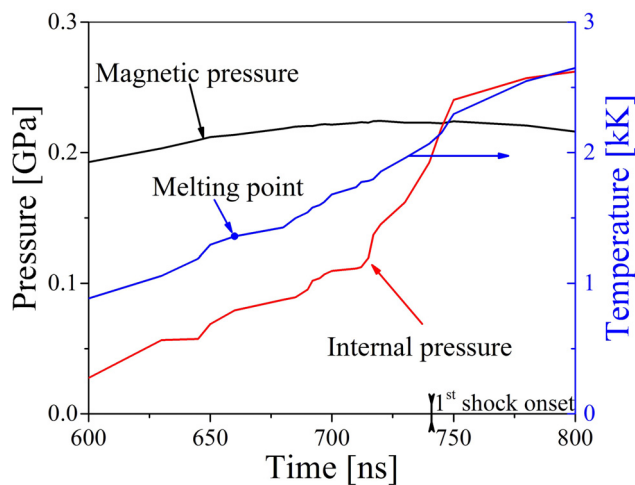


FIG. 5. Temporal evolution of the magnetic pressure (black), temperature (blue) and internal pressure (red) at the exploding Cu wire surface.

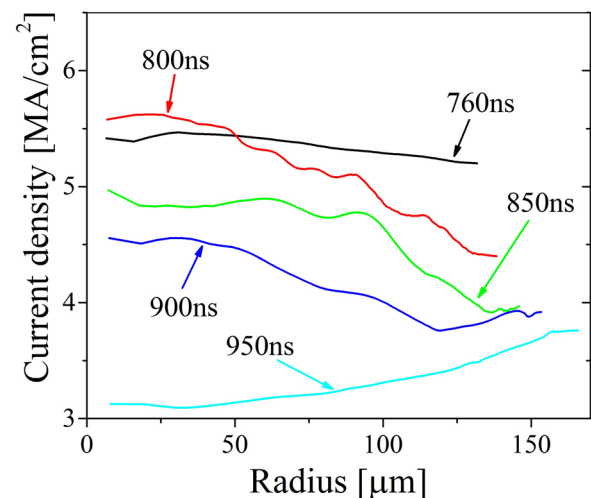


FIG. 6. Simulated radial distributions of the current density at different times of the Cu wire explosion.

Rough estimates showed that this effect should lead to a time delay in the second shock appearance relative to the onset of the first shock of ~ 160 ns, which roughly agrees with the experimental data.

B. Aluminum wire explosion

Analysis of the Al wire explosion was carried out using the same 1D MHD model coupled with EOS for water and Al, and the QLMD conductivity model.⁴¹ It was found that both the EOS for Al and the conductivity model should be corrected in order to obtain the best fit between the simulation and the experimental results. The approach, which was used to correct the EOS and conductivity model, was the same as that used for the Cu wire explosion. The experimentally obtained and simulated waveforms of the discharge current, resistive voltage, and channel expansion are shown in Figs. 7(a)–7(c). One can see a satisfactory agreement between the experimental and simulated data. Let us note that similarly to Cu wire explosions, the wire's radial expansion could not be resolved during the period 650–1250 ns because the generated strong shock wave screens the exploded wire. The simulated current density radial distributions at different times are shown in Fig. 7(d). One can see that at $t \leq 300$ ns, the skin effect is relatively pronounced.

The measured energy density deposited into the wire by the time of the onset of the first weak shock ($t \approx 490$ ns) was found to be almost equal to the energy density, which one requires to heat the entire wire up to T_m^{Al} plus the enthalpy of fusion. This correlates well with the results of 1D MHD

simulations where the melting temperature was reached at $t \approx 500$ ns. Note, that for Al, in contrast to Cu wire explosions, the magnetic pressure does not influence the onset of the first weak shock. Indeed, 1D MHD simulations showed that the internal pressure of the Al wire exceeds the magnetic pressure prior to this transition due to significantly faster energy density deposition, than for Cu wire explosions. Namely, the energy density deposition rate for Al wire explosions differs from that of Cu wire explosions by a factor of 9 at $t \approx 490$ ns and by a factor of 6 at $t \approx 740$ ns. More details can be found in Fig. 8 where the time-dependent energy density deposition rates for Cu and Al wire explosions are presented.

The onset of the second weak shock was obtained at $t \approx 600$ ns, which precedes by ~ 260 ns the time when the energy density deposited into the wire reaches the value necessary for the vaporization of the entire wire. Indeed, at $t \approx 600$ ns, the energy density deposition into the wire was ~ 1.3 kJ/g which is insufficient even to heat the entire wire to its boiling temperature T_b^{Al} . The latter is qualitatively similar to Cu wire explosions where it was found that the onset of the second weak shock corresponds to the beginning of the evaporation process. The vaporization process of the Al wire can be characterized by the temporal and spatial evolution of the current density's radial distribution (see Fig. 9) showing wave-like propagation of the maximum of the current density from the wire periphery towards the axis with a typical velocity of ~ 700 m/s. Namely, at $t \approx 600$ ns, when second weak shock separates from the wire, there is a decrease in the conductivity at the wire's periphery related to liquid-

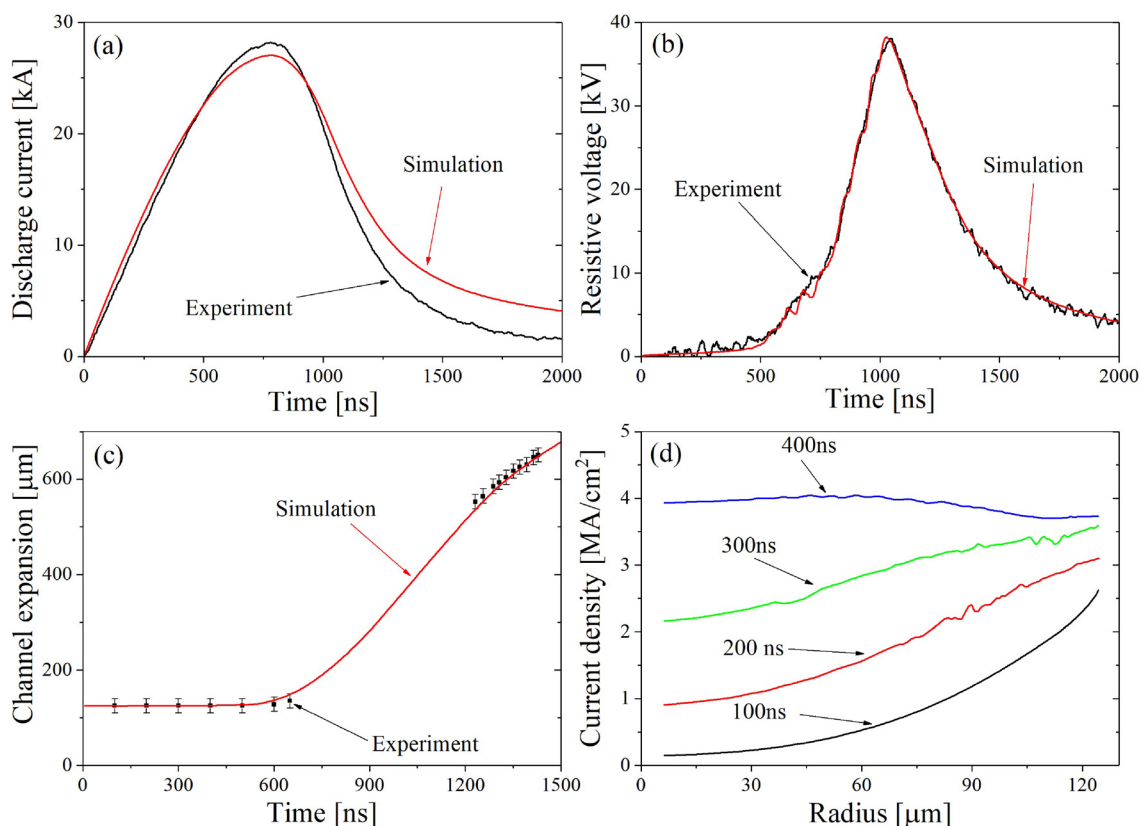


FIG. 7. Experimental and simulated waveforms of the discharge current (a), resistive voltage (b), channel expansion (c), and simulated current density radial distribution (d) for Al wire explosion.

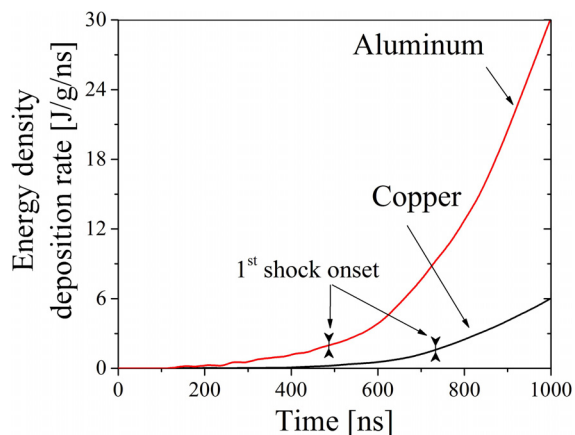


FIG. 8. Energy density deposition rate as a function of time for Cu and Al wires.

vapor phase transition, which leads to the increase in the current density through neighboring radial shells. These results confirm the numerical analysis of wire explosions described in Refs. 21 and 41 and predict the evaporation wave propagating from the wire periphery towards the axis.

For Al wire electrical explosions using generator #2, qualitatively similar results were obtained. Namely, the onset of the first weak shock was found at the time when the deposited energy density becomes almost equal to the sum of the energy density needed to heat the wire to its melting temperature plus the enthalpy of fusion. Also, the onset of the second weak shock was found at the time when only a fraction of the wire can experience vaporization.

C. Tungsten wire explosion

Underwater electrical explosions of W wires were not analyzed using 1D MHD simulations because of the absence of a conductivity model required to be coupled to the simulation. W wire explosions are characterized by very different discharge current and resistive voltage waveforms compared to those for Cu and Al (see Fig. 2). A long duration plateau of the current and voltage waveforms can be related to different phase transition durations during the explosion.

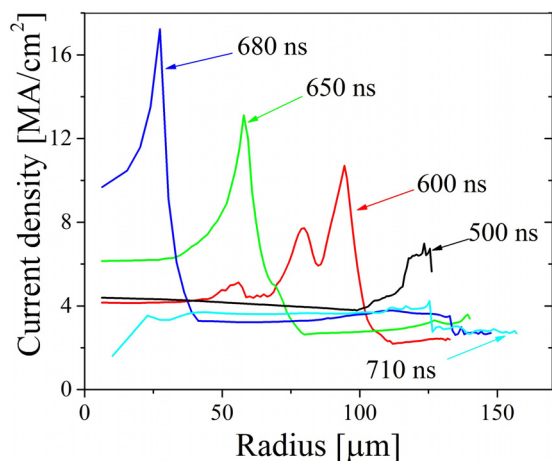


FIG. 9. Simulated radial distributions of the current density at different times of the Al wire explosions.

Considering that the onset of the first weak shock is related to solid \rightarrow liquid phase transition, one can consider that the current and voltage plateaus occur during the liquid phase. The latter is characterized by an almost constant wire conductivity, σ^0 , which can be inspected by semi-empirical conductivity in the melting phase in the temperature range of 3695–6203 K:²²
$$\sigma(\rho, T) = \frac{\sigma^0 [1 - \alpha(T)(T - T^0)]}{1 + \beta(T - T^0)},$$
 where σ^0 , ρ^0 , and T^0 are the conductivity, density, and temperature at the melting point, respectively, $\beta \approx 2 \times 10^{-5} \text{ K}^{-1}$ is the thermal coefficient of conductivity for the liquid metal and $\alpha \approx 4.4 \times 10^{-4} \text{ K}^{-1}$ is the thermal expansion coefficient. In addition, we confirm the results described in Ref. 24 regarding the correspondence of the first maximum in the resistive voltage to the time when melting of the W wire should occur. An insignificantly earlier (~ 60 ns) onset of the first weak shock wave with respect to the voltage maximum obtained in our experiments can be related to the different wire diameters, pulse power generators, and medium for which the wire explosion was studied.

The normalized W resistance R/R_0 , where R_0 is the resistance for normal conditions (solid phase, room temperature) as a function of the deposited energy density is shown in Fig. 10. This result agrees well with the data presented in Ref. 52. The linear part of this dependence⁶ for deposited energy densities $\varepsilon \leq 1 \text{ kJ/g}$ can be approximated as $R/R_0 = 1 + \beta\varepsilon$, where $\beta \approx 0.025 \text{ J/g}$. At larger deposited energies, one obtains the W liquid phase characterized by an almost constant conductivity up to a deposited energy density of $\sim 7 \text{ kJ/g}$. A further increase in the deposited energy density leads to the beginning of wire vaporization and a corresponding increase in the resistance.

Similarly to Al, W wire explosions using generator #2 were found to be qualitatively comparable to the results described above for generator #1. Namely, the first disturbance obtained in the water cannot be related to wire melting because of the very low energy deposited up to that time (9 times less than that needed for the entire wire melting). This disturbance can be explained by fast desorption of absorbed surface layer gases. The onset of the first weak shock was

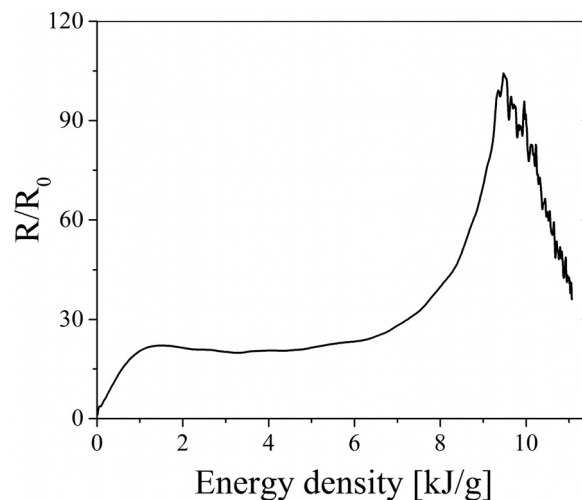


FIG. 10. Normalized resistance versus energy density deposited into the W wire.

obtained ~ 30 ns after the current maximum at a time when the deposited energy was $\sim 15\%$ smaller than the energy density required for the heating and melting of the entire wire. The onset of the second weak shock is also obtained at a time when the deposited energy is significantly smaller than that required for entire wire vaporization. Thus, one can conclude that the onset times of the first and second weak shock waves occur when the wire is only partially melted or vaporized.

V. SUMMARY

High resolution space- and time-resolved streak images of microsecond timescale underwater electrical explosions of single Cu, Al, and W wires showed the generation of two weak shock waves preceding a strong shock wave generation at the time when the vapor-low-ionized plasma phase transition occurs. It was shown that for Al and partially for W wire explosions, the onset of the first weak shock wave was associated with the melting of the entire wire, which agrees well with the energy density deposited into the wire sufficient for this process. Moreover, we show that in general one cannot relate the generation of weak shocks with the phase transition of the entire wire.

For Cu wire explosions using generator #1, the onset of the first weak shock was obtained at the time when the energy density deposited into the wire was almost two-fold larger than the energy density needed to heat the wire to its melting point plus the enthalpy of fusion. Using a 1D MHD simulation, this result was explained by magnetic pressure which suppressed the wire's expansion until the internal pressure of the wire is high enough.

The onset of the second weak shock wave was found to be related to the beginning of the vaporization of the wires, meaning, that its appearance is not related to the evaporation of the entire wire. Namely, Cu, Al, and W wires explosions consistently showed that the energy density deposited into the wires prior to the onset of the second shock wave was lower than the energy density needed to evaporate the entire wire. For the cases of Cu and Al wire explosions, 1D MHD simulation showed the beginning of vaporization of the wire at its periphery at the onset of the second weak shock and propagation of a vaporization wave towards the axis of the wire. For W wire explosion, the obtained data confirmed earlier obtained results^{22,24} regarding the melting point of the wire, the conductivity plateau at the liquid phase, and the action integral⁶⁻⁸ required to obtain the wire explosion. The results for Al and W wire explosions obtained in experiments with generator #2 were qualitatively similar. Only, for Cu wire explosions, a pronounced skin effect leads to the onset of the first shock wave at a time when only partial wire melting occurs.

ACKNOWLEDGMENTS

We thank Dr. J. Leopold for critical reading of this manuscript and E. Flyat for generous technical assistance. This research was supported by the Center for Absorption in Science, Ministry of Immigrant Absorption, State of Israel.

- ¹V. E. Fortov and I. T. Iakubov, *The Physics of Non-Ideal Plasma* (World Scientific, Singapore, 2000).
- ²*Exploding Wires*, edited by W. G. Chase and H. K. Moore (Plenum, NY, 1959), Vol. 1-4.
- ³I. M. Vitkovitsky, *High Power Switching* (Van Nostrand Reinhold, Florence, Kentucky, USA, 1987).
- ⁴F. D. Bennett, "High temperature exploding conductors," in *Progress in High Temperature Physics and Chemistry* (Pergamon Press, Oxford, 1968).
- ⁵S. V. Lebedev and A. I. Savvatimskii, *Sov. Phys. Usp.* **27**, 749 (1984).
- ⁶V. A. Burtsev, N. V. Kalinin, and A. V. Luchinskii, *Electrical Explosion of Conductors and Its Applications* (Energoizdat, Moscow, 1990) [in Russian].
- ⁷G. A. Mesyats, *Cathode Phenomena in a Vacuum Discharge: The Breakdown, the Spark and the Arc* (Nauka, Moscow, 2000).
- ⁸G. A. Shneerson, M. I. Dolotenko, and S. I. Krivosheev, *Strong and Super-Strong Pulsed Magnetic Fields Generation* (Walter de Gruyter GmbH, Berlin/Boston, 2014).
- ⁹S. Sedoi, G. A. Mesyats, V. I. Oreshkin, V. V. Valevich, and L. I. Chemezova, *IEEE Trans. Plasma Sci.* **27**, 845 (1999).
- ¹⁰A. A. Neuber, "Explosive driven pulsed power," in *Helical Magnetic Flux Compression Generators* (Springer-Verlag-Berlin, Heidelberg, 2005).
- ¹¹V. I. Oreshkin, *Phys. Plasmas* **15**, 092103 (2008).
- ¹²S. A. Chaikovsky, V. I. Oreshkin, I. M. Datsko, N. A. Labetskaya, and N. A. Ratakhin, *Phys. Plasmas* **21**, 042706 (2014).
- ¹³G. S. Sarkisov, S. E. Rosenthal, K. W. Struve, and D. H. McDaniel, *Phys. Rev. Lett.* **94**, 035004 (2005).
- ¹⁴S. A. Pikuz, T. A. Shelkovenko, D. B. Sinars, J. B. Greenly, Y. S. Dimant, and D. A. Hammer, *Phys. Rev. Lett.* **83**, 4313 (1999).
- ¹⁵D. B. Sinars, M. Hu, K. M. Chandler, T. A. Shelkovenko, S. A. Pikuz, J. B. Greenly, D. A. Hammer, and B. R. Kusse, *Phys. Plasmas* **8**, 216 (2001).
- ¹⁶G. S. Sarkisov, S. E. Rosenthal, K. W. Struve, V. V. Ivanov, E. E. Cowan, A. Astanovitskiy, and A. Haboub, *Phys. Plasmas* **14**, 052704 (2007).
- ¹⁷P. P. Malushevskii, *Basics of Pulsed Discharge Technology* (Naukova Dumka, Kiev, 1983) [in Russian].
- ¹⁸E. V. Krivitskii, *Dynamics of Electrical Explosion in Liquid* (Naukova Dumka, Kiev, 1983) [in Russian].
- ¹⁹V. T. Gurovich, A. Grinenko, Y. E. Krasik, and J. Felsteiner, "Simplified model of underwater electrical discharge," *Phys. Rev. E* **69**, 036402 (2004).
- ²⁰G. V. Ivanenkov, S. A. Pikuz, T. A. Shelkovenko, V. M. Romanova, I. V. Glazirin, O. G. Kotova, and A. N. Slesareva, in *Review of the Literature on Modeling of Electrical Explosion of Thin Metal Wires*, edited by P. N. Lebedev (Physics Institute of the Russian Academy of Sciences, Moscow, 2005), Vol. 11 [in Russian].
- ²¹S. I. Tkachenko, K. V. Khishchenko, V. S. Vorob'ev, P. R. Levashov, I. V. Lomonosov, and V. E. Fortov, *High Temperature* **39**, 674 (2001).
- ²²N. I. Kuskova, S. I. Tkachenko, and S. V. Koval, *J. Phys.: Condens. Matter* **9**, 6175 (1997).
- ²³W. DeSilva and J. D. Katsouris, *Phys. Rev. E* **57**, 5945 (1998).
- ²⁴I. V. Oreshkin, R. B. Baksht, A. Y. Labezki, A. G. Roussikh, A. V. Shishlov, P. R. Levashov, K. V. Khishchenko, and I. V. Glazyrin, *Tech. Phys.* **49**, 843 (2004).
- ²⁵S. I. Tkachenko, V. S. Vorob'ev, and S. P. Malysenko, *J. Phys. D: Appl. Phys.* **37**, 495 (2004).
- ²⁶A. Grinenko, Y. E. Krasik, S. Efimov, A. Fedotov, V. T. Gurovich, and I. Oreshkin, *Phys. Plasmas* **13**, 042701 (2006).
- ²⁷D. Sheftman and Y. E. Krasik, *Phys. Plasmas* **17**, 112702 (2010).
- ²⁸D. Sheftman and Y. E. Krasik, *Phys. Plasmas* **18**, 092704 (2011).
- ²⁹D. Sheftman, D. Shafer, S. Efimov, and Y. E. Krasik, *Phys. Plasmas* **19**, 034501 (2012).
- ³⁰J. Stephens, J. Dickens, and A. Neuber, *Phys. Rev. E* **89**, 053102 (2014).
- ³¹K.-J. Chung, K. Lee, Y. S. Hwang, and D.-K. Kim, *J. Appl. Phys.* **120**, 203301 (2016).
- ³²A. Virozub, V. T. Gurovich, D. Yanuka, O. Antonov, and Y. E. Krasik, *Phys. Plasmas* **23**, 092708 (2016).
- ³³National Technical Information Service Document No. DE85014241 (S. P. Lyon and J. D. Johnson, *Sesame: The Los Alamos National Laboratory Equation-of-State Database*, LANL Rep. LA UR-92-3407, 1992). Copies may be ordered from the National Technical Information Service, Springfield, VA, 22161.
- ³⁴A. V. Bushman and V. E. Fortov, *Sov. Technol. Rev. B* **1**, 219 (1987).
- ³⁵R. M. More, K. H. Warren, D. A. Young, and G. B. Zimmerman, *Phys. Fluids* **31**, 3059 (1988).

- ³⁶Y. D. Bakulin, V. F. Kuropatenko, and A. V. Luchinskii, *Zh. Tekh. Fiz.* **46**, 1963 (1976).
- ³⁷Y. T. Lee and R. M. More, *Phys. Fluids* **27**, 1273 (1984).
- ³⁸R. Redmer, *Phys. Rev. E* **59**, 1073 (1999).
- ³⁹M. P. Desjarlais, *Contrib. Plasma Phys.* **41**, 267 (2001).
- ⁴⁰M. P. Desjarlais, J. D. Kress, and L. A. Collins, *Phys. Rev. E* **66**, 025401 (2002).
- ⁴¹A. E. Ter-Oganesyan, S. I. Tkachenko, V. M. Romanova, A. R. Mingaleev, T. A. Shelkovenko, and S. A. Pikuz, *Plasma Phys. Rep.* **31**, 919 (2005).
- ⁴²A. G. Russkikh, V. I. Oreshkin, A. Y. Labetsky, S. A. Chaikovsky, and A. V. Shishlov, *Tech. Phys.* **52**, 571 (2007).
- ⁴³Y. E. Krasik, A. Grinenko, A. Sayapin, S. Efimov, A. Fedotov, V. T. Gurovich, and V. I. Oreshkin, *IEEE Trans. Plasma Sci.* **36**, 423 (2008) and references therein.
- ⁴⁴Y. E. Krasik, S. Efimov, D. Sheftman, A. Fedotov-Gefen, O. Antonov, D. Shafer, D. Yanuka, M. Nitishinskiy, M. Kozlov, L. Gilburd, G. Toker, S. Gleizer, E. Zvulun, V. T. Gurovich, D. Varentsov, and M. Rodionova, *IEEE Trans. Plasma Sci.* **44**, 412 (2016).
- ⁴⁵A. Grinenko, A. Sayapin, V. T. Gurovich, S. Efimov, J. Felsteiner, and Y. E. Krasik, *J. Appl. Phys.* **97**, 023303 (2005).
- ⁴⁶A. Sayapin, A. Grinenko, S. Efimov, and Y. E. Krasik, *Shock Waves* **15**, 73 (2006).
- ⁴⁷D. Yanuka, A. Rososhek, and Y. E. Krasik, *Phys. Plasmas* **24**, 053512 (2017).
- ⁴⁸O. Antonov, S. Efimov, D. Yanuka, M. Kozlov, V. T. Gurovich, and Y. E. Krasik, *Appl. Phys. Lett.* **102**, 124104 (2013).
- ⁴⁹*NIST Chemistry WebBook, NIST Standard Reference Database Number 69*, edited by P. J. Linstrom and W. G. Mallard (National Institute of Standards and Technology, Gaithersburg, MD, 2001), p. 20899 (last accessed May 28, 2018).
- ⁵⁰G. K. White and S. J. Collocott, *J. Phys. Chem. Ref. Data* **13**, 1251 (1984).
- ⁵¹T. E. Pochapsky, *Acta Metall.* **1**, 747 (1953).
- ⁵²V. N. Korobenko, A. D. Rakhel, A. I. Savvatimskiy, and V. E. Fortov, *Plasma Phys. Rep.* **28**(12), 1008–1016 (2002).